Spectral analysis for elastica dynamics in a shear flow

Lujia Liu, Paweł Sznajder, and Maria L. Ekiel-Jeżewska*
*Institute of Fundamental Technological Research Polish Academy of Sciences,
Pawińskiego 5b, 02-106 Warsaw, Poland*

We present the spectral analysis of three-dimensional dynamics of an elastic filament in a shear flow of a viscous fluid at a low Reynolds number in the absence of Brownian motion. The elastica model is used. The fiber initially is almost straight at an arbitrary orientation, with small perpendicular perturbations in the shear plane and out-of-plane. To analyze the stability of both perturbations, equations for the eigenvalues and eigenfunctions are derived and solved by the Chebyshev spectral collocation method. It is shown that their crucial features are the same as in the case of the two-dimensional elastica dynamics in shear flow [Becker and Shelley, Phys. Rev. Lett. **87**, 198301 (2001)] and the three-dimensional elastica dynamics in the compressional flow [Chakrabarti *et al.*, Nat. Phys. **16**, 689 (2020)]. We find a similar dependence of the buckled shapes on the ratio of bending to hydrodynamic forces as in the simulations for elastic fibers of a nonzero thickness [Słowicka *et al.*, New J. Phys. **24**, 013013 (2022)].

I. INTRODUCTION

Dynamics of flexible micro and nanoobjects in fluid flows have been recently widely investigated theoretically, numerically, and experimentally [1–26]. The interest is motivated by potential applications to microorganisms (e.g., diatoms [27], bacteria [15], cells [19], or actin [18,25]), and to artificially produced micro and nanofibers [17,20].

For elastic filaments, typical time-dependent shape deformations and orientations have been analyzed for different values of the bending stiffness and aspect ratio. Various theoretical approaches have been used [2], including the bead models [21,28,29]. Buckling of elastic filaments has been studied in various fluid flows: extensional [15,22,26], cellular [12,14,23,24], stagnation point [16], corner [30], shear [4,5,10], and unidirectional [31].

Many articles have focused on flexible filaments in shear flows [18,19,25,27,29,32–38]. The buckling instability of slender fibers located in the shear plane has been derived from the two-dimensional spectral analysis of the elastica [10]. The eigenvalues have been evaluated for a wide range of values of the elastoviscous number [10].

The goal of this work is to analyze the stability of elastica (i.e., infinitely thin elastic fiber described by a local slender body theory) in a shear flow by solving a three-dimensional spectral problem: not only for in-plane but also for out-of-plane perturbations. Using the Chebyshev collocation method [39], we evaluate the eigenvalues and eigenfunctions and discuss the results.

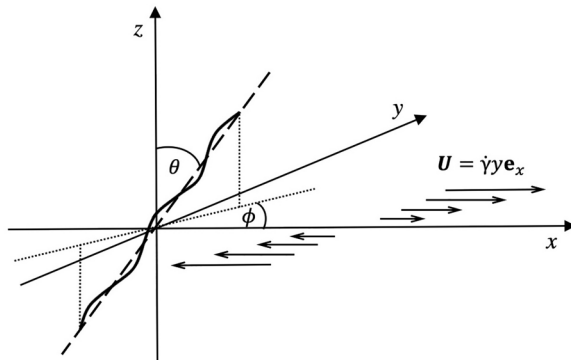*Corresponding author: mekiel@ippt.pan.pl

FIG. 1. A schematic of a slender particle in a shear flow.

II. SYSTEM AND THEORETICAL MODEL

A slender elastic filament is immersed in a shear flow $\tilde{U} = (\dot{\gamma} y, 0, 0)$ of a fluid with the dynamic viscosity μ. The ratio of the radius R of the particle cross-section to its length L is much smaller than unity, i.e., $R/L \ll 1$. The filament is assumed to be inextensible, and its length L is used as the unit of length. The dimensionless position of the filament centerline is denoted as $\boldsymbol{x}(s, t)$, where $s \in [-1/2, 1/2]$ is the arclength coordinate of a filament segment and t is time. Owing to the filament inextensibility, $\boldsymbol{x}_s \cdot \boldsymbol{x}_s = 1$. Here we ignore gravitational effects, Brownian forces, and fluid inertia; only elastic and viscous forces are considered to result in the filament dynamics following from the incompressible Stokes equations.

For the elastic forces, we apply the inextensible Euler-Bernoulli beam model [40]. For the dynamics, we use the local simple beam model of the slender-body theory [1,41–43]. In this simple local model, the long-range hydrodynamic interactions of fiber segments and the effects of the fiber thickness are not taken into account, and the dynamics of fibers aligned with the flow cannot be determined. Nevertheless, the advantage of this model is its simplicity, which allows us to analyze theoretically the fiber stability.

With the length unit L, the time unit $\dot{\gamma}^{-1}$ and $\boldsymbol{U} = \tilde{U}/(\dot{\gamma} L)$, the dimensionless elastica three-dimensional (3D) governing equation is [1,10,16,44,45],

$$\eta(2\boldsymbol{I} - \boldsymbol{x}_s \boldsymbol{x}_s) \cdot [\boldsymbol{x}_t - \boldsymbol{U}(\boldsymbol{x})] = [T(s, t)\boldsymbol{x}_s]_s - \boldsymbol{x}_{ssss}, \tag{1}$$

where $T(s, t)$ represents the tension in the filament at point s and time t, $\boldsymbol{I}$ in a unit 3×3 matrix, and η denotes the elastoviscous number,

$$\eta = \frac{2\pi \mu \dot{\gamma} L^4}{EJ \ln(L/R)}, \tag{2}$$

defined as the ratio of the viscous drag to the elastic restoring forces [16], with Young's modulus E of the filament, and its area moment of inertia $J = \pi R^4/4$.

In this work, we assume that the particle is slightly deformed from a straight shape at a certain orientation, described by the azimuthal and polar angles, $\phi(t)$ and $\theta(t)$, as shown in Fig. 1. The azimuthal angle deals with the projection onto the shear plane (x, y), i.e., the plane spanned by the directions of the flow and the flow gradient. Owing to symmetries, we can restrict to $0 \leqslant \phi \leqslant \pi$ and $0 \leqslant \theta \leqslant \pi/2$ without loss of generality.

The position vector $\boldsymbol{x}(s, t)$ can be described by

$$\boldsymbol{x} = s\boldsymbol{\lambda} + u\boldsymbol{\lambda}_i + v\boldsymbol{\lambda}_o, \tag{3}$$

where $u(s, t)$ and $v(s, t)$ are, respectively, the in-plane and out-of-plane deflections relative to a straight rod with the orientation (shown as a dashed line in Fig. 1) determined by the unit vector

$$\boldsymbol{\lambda} = (\cos\phi\sin\theta, \, \sin\phi\sin\theta, \, \cos\theta). \tag{4}$$

In Eq. (3), the in-plane (x, y) and out-of-plane unit vectors perpendicular to $\boldsymbol{\lambda}$ are $\boldsymbol{\lambda}_i = (-\sin\phi, \cos\phi, 0)$ and $\boldsymbol{\lambda}_o = (-\cos\phi\cos\theta, -\sin\phi\cos\theta, \sin\theta)$, respectively.

The motivation of the assumption (3) is the following. If an elastic fiber is straight in elastic equilibrium, it seems realistic to expect that in some experiments the fibers would be initially straight (assuming that the shear flow is switched on at a certain time). For example, such a situation took place in the experiments in Refs. [29,37]. Therefore, it makes sense to consider small perturbations (caused by the shear flow) from a straight elastic fiber.

III. ELASTICA EQUATIONS FOR SMALL 3D PERTURBATIONS FROM AN ARBITRARY ORIENTATION

We assume that both perturbations, u and v, are small and of the same order. Then, we insert the expression (3) into Eq. (1) and perform a formal expansion of Eq. (1) in powers of u and v, up to the first order. We obtain a set of linearized equations. In this section, we present the zero-order and first-order equations.

Expanding the governing elastica equation (1), for $u = v = 0$ one obtains the following zero-order equations:

$$\dot{\phi} = -\sin^2\phi, \tag{5}$$

$$\dot{\theta} = \tfrac{1}{4}\sin(2\phi)\sin(2\theta), \tag{6}$$

$$T = -\frac{\eta}{4}\sin^2\theta\sin(2\phi)\left(s^2 - \frac{1}{4}\right), \tag{7}$$

with the assumed boundary condition $T = 0$ at the ends of the filament, i.e., for $s = \pm 1/2$. By solving Eq. (5), one obtains

$$\cot\phi(t) = t + B, \tag{8}$$

and by combining Eq. (6) with Eq. (5), one gets $\theta(t) = 0$ or π, and otherwise

$$\tan\theta(t) = \frac{C}{\sin\phi(t)}, \tag{9}$$

where B and C are constants dependent on the initial conditions. The zero-order motion of elastica corresponds to the Jeffery orbit [46] in the limit of an infinitely thin rigid rod (the aspect ratio $\ell \to \infty$). In this limit, the time to approach (or leave) $\phi = 0$ or π is infinite, and therefore an elastica does not tumble, and as such, it can approximate dynamics of a fiber with a nonzero thickness only for the angle ϕ not very close to zero or π [29,35][1]. However, Jeffery trajectories $\theta(\phi)$ of the elastica zero-order motion and of a rigid rod with a sufficiently large aspect ratio, e.g., $\ell \gtrsim 100$, are very close to each other, as illustrated in Fig. 2.

Further, the first-order equations are derived from Eq. (1). The in-plane perturbation u satisfies the following equation:

$$u_{ssss} + 2\eta u_t + \eta\sin(2\phi)u + \eta\sin(2\phi)\sin^2\theta s u_s + \frac{\eta}{4}\sin(2\phi)\sin^2\theta\left(s^2 - \frac{1}{4}\right)u_{ss} = 0. \tag{10}$$

---

[1]To include the effects of the fiber thickness, the expansion can be performed to higher orders in the slenderness parameter $2R/L$ [47,48].
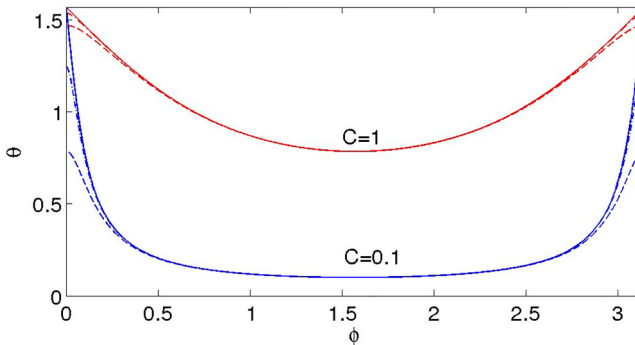
FIG. 2. Jeffery orbits $\theta(\phi)$ in a shear flow for spheroids with the aspect ratios $\ell = 10$ (dashed line) and $\ell = 30$ (dash-dotted line) [46] and for the zero-order elastica, Eq. (9) (solid line). The corresponding values of C as indicated.

The equation for the out-of-plane perturbation v has the form

$$v_{ssss} + 2\eta v_t - \eta \sin(2\phi)\cos^2\theta v + 2\eta \cos(2\phi)\cos(\theta)u$$

$$+\eta \sin(2\phi)\sin^2\theta s v_s + \frac{\eta}{4}\sin(2\phi)\sin^2\theta\left(s^2 - \frac{1}{4}\right)v_{ss} = 0. \tag{11}$$

In the considered system, there are no external torques exerted on the filament ends

$$u_{ss} = v_{ss} = 0 \text{ at } s = \pm\tfrac{1}{2}, \tag{12}$$

and external forces on the filament ends vanish

$$u_{sss} = v_{sss} = 0 \text{ at } s = \pm\tfrac{1}{2}. \tag{13}$$

We remind that the slender body theory used in the above equations neglects the end contribution at the leading order in slenderness considered. This property and a possible generalization are discussed, e.g., in Sec. 4.2 of Ref. [36].

In principle, evolution equations for the perturbations u and v could be solved numerically, with the initial condition $u = v = 0$. However, in this work we do not do it. Instead, we consider the spectral problem that gives information about the stability of the perturbations, as described in the next sections.

IV. EIGENPROBLEM AND STABILITY OF SMALL 3D PERTURBATIONS FROM AN ARBITRARY ORIENTATION

To estimate the stability of the in-plane (u) and out-of-plane (v) perturbations, we consider the following eigenproblem, which is a 3D generalization of the in-plane study [10], and in the next section will be solved by the Chebyshev spectral collocation method [39,49], also applied in Refs. [10,26]. We follow the standard assumption that

$$\{u, v\} = \{\Phi_u(s)\exp(\sigma t), \Phi_v(s)\exp(\sigma t)\}, \tag{14}$$

where Φ_u and Φ_v are shapes of the in- and out-of-plane perturbations and σ is the complex growth rate. It is important to stress that, for the stability analysis, we consider $\Phi_u(s)$ and $\Phi_v(s)$ as functions of s only, independent of time t. Therefore, for the stability analysis, we consider arbitrary orientation angles θ and ϕ in Eq. (3), regardless the zeroth-order equations from the previous section.

The expression (14) is inserted into Eqs. (10) and (11), which results in the following spectral problem:

$$2\eta\left(\sigma + \frac{\sin(2\phi)}{2}\right)\Phi_u = \mathcal{L}[\Phi_u], \tag{15}$$

$$2\eta(\sigma - \frac{\sin(2\phi)}{2}\cos^2\theta)\Phi_v = \mathcal{L}[\Phi_v] - 2\eta\cos(2\phi)\cos\theta\,\Phi_u, \tag{16}$$

where $\mathcal{L}$ denotes the differential operator

$$\mathcal{L} = -\frac{\partial^4}{\partial s^4} - \frac{\eta}{4}\left(s^2 - \frac{1}{4}\right)\sin(2\phi)\sin^2\theta\frac{\partial^2}{\partial s^2} - \eta s\sin(2\phi)\sin^2\theta\frac{\partial}{\partial s}, \tag{17}$$

and the boundary conditions follow from Eqs (12) and (13).

V. SPECTRUM AND EIGENFUNCTIONS FOR SMALL PERTURBATIONS FROM THE SHEAR PLANE

In this section, we consider the eigenproblem for the in-plane and out-of-plane perturbations when

$$\theta = \pi/2. \tag{18}$$

In this case, the last term in Eq. (16) vanishes, which means that there is no coupling between Φ_u and Φ_v. Therefore, we now assume

$$\{u, v\} = \{\Phi_u(s)\exp(\sigma_u t), \Phi_v(s)\exp(\sigma_v t)\}, \tag{19}$$

with, in general, different exponents σ_u and σ_v for the in-plane and out-of-plane perturbations, respectively.

The spectral problem for the in-plane perturbations at $\theta = \pi/2$ was solved by Becker and Shelley [10] who were interested in this special case because, for an almost straight elastic filament performing a Jeffery orbit in the plane of shear, i.e., at $\theta = \pi/2$, the hydrodynamic forces exerted on it by the fluid are the largest.

Here we extend the results from Ref. [10] by taking into account not only in-plane, but also out-of-plane perturbations Φ_u and Φ_v, respectively. In the case of $\theta = \pi/2$, with the ansatz (19), the first-order Eqs (15) to (17) for the exponentially growing perturbations (14) are replaced by

$$2\eta\left(\sigma_u + \frac{\sin(2\phi)}{2}\right)\Phi_u = \tilde{\mathcal{L}}[\Phi_u], \tag{20}$$

$$2\eta\sigma_v\Phi_v = \tilde{\mathcal{L}}[\Phi_v], \tag{21}$$

with

$$\tilde{\mathcal{L}} = -\frac{\partial^4}{\partial s^4} - \frac{\eta\sin(2\phi)}{4}\left(s^2 - \frac{1}{4}\right)\frac{\partial^2}{\partial s^2} - \eta\sin(2\phi)s\frac{\partial}{\partial s}. \tag{22}$$

Equations (20) and (21) for the in-plane and out-of-plane perturbations are decoupled from each other. The eigenfunction Φ_u belonging to an eigenvalue σ_u is identical to the eigenfunction Φ_v belonging to the shifted eigenvalue $\sigma_u + \sin(2\phi)/2$. Therefore, we focus on the solutions to Eqs. (20) and (22). The generalization for the out-of-plane perturbations is straightforward.

We solve the eigenvalue problem for Φ_u, defined by Eqs. (20) and (22), by the Chebyshev spectral collocation method [39,49]. The calculated eigenspectrum for the in-plane perturbation Φ_u is demonstrated in the left panel of Fig. 3. The largest eigenvalue (blue line) agrees well with the result presented in Fig. 2 of Ref. [10]. In this work, we perform a more detailed new analysis: we evaluate not only the single largest eigenvalue, but the eight largest consecutive eigenvalues σ_u and plot them in Fig. 3.
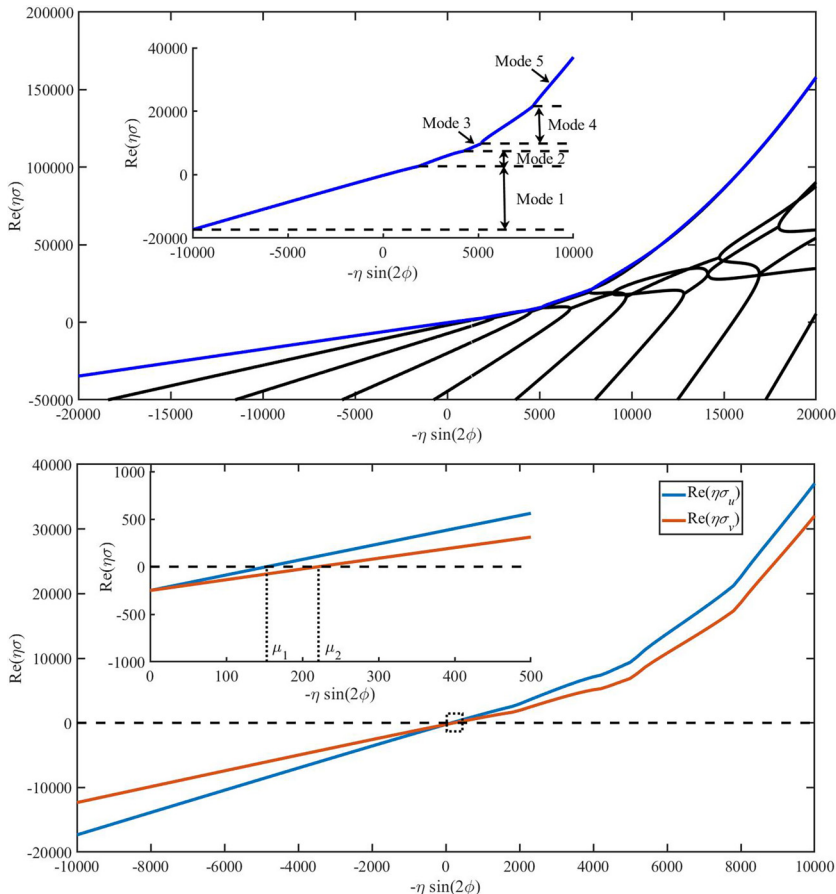
FIG. 3. The real part of the eigenspectrum $\eta\sigma$ as a function of $-\eta\sin(2\phi)$. Top: Up to eight largest eigenvalues $\eta\sigma \equiv \eta\sigma_u$ (black and blue). The largest eigenvalue, shown in blue, extends the range of the calculations shown in Fig. 2 in Ref. [10]. Bottom: The largest eigenvalues, $\eta\sigma_u$ and $\eta\sigma_v$, for the in-plane (blue) and out-of-plane (red) perturbations Φ_u and Φ_v, respectively.

The modes 1 to 5 are the most unstable eigenfunctions Φ_u for the range of the smallest positive eigenvalues σ_u. These most unstable eigenvalues in this range (but not their eigenfunctions) are shown in Fig. 2 of Ref. [10] and also in our Fig. 3. The modes 1 to 5 appear for $153.2 \leqslant -\eta\sin(2\phi) \leqslant 10^4$. Their shapes are presented in the top panel of Fig. 4, using colors. The eigenfunctions Φ_u are normalized in such a way that $\max_s[\Phi_u(s)] = 1$. In the bottom panel of Fig. 4, shapes of the most unstable eigenfunctions Φ_u are shown for the whole range $0 \leqslant -\eta\sin(2\phi) \leqslant 6 \times 10^4$.

The eigenfunctions Φ_u corresponding to the most unstable eigenvalues are even for modes 1, 3, and 4, and odd for modes 2 and 5. In general, for certain values of $-\eta\sin(2\phi)$ they are odd, as the examples shown in the top panel of Fig. 5; for other values they are even, as the examples visible in the bottom panel of Fig. 5. At larger values of $-\eta\sin(2\phi)$, there appear buckling modes with larger wavenumbers. This finding seems to agree with more buckled shapes observed in the numerical simulations with the decreased bending stiffness, as shown in Fig. 12 of Ref. [29].

For stability analysis, the most important is the largest eigenvalue. In the bottom panel of Fig. 3, the largest eigenvalues for the in-plane and out-of-plane perturbations are compared with each other. The eigenspectrum for Eq. (21), i.e., for perturbations Φ_v perpendicular to the shear plane, corresponds to $\eta\sigma_v = \eta\sigma_u + \eta\sin(2\phi)/2$. Therefore, the growth rate of the most unstable out-of-
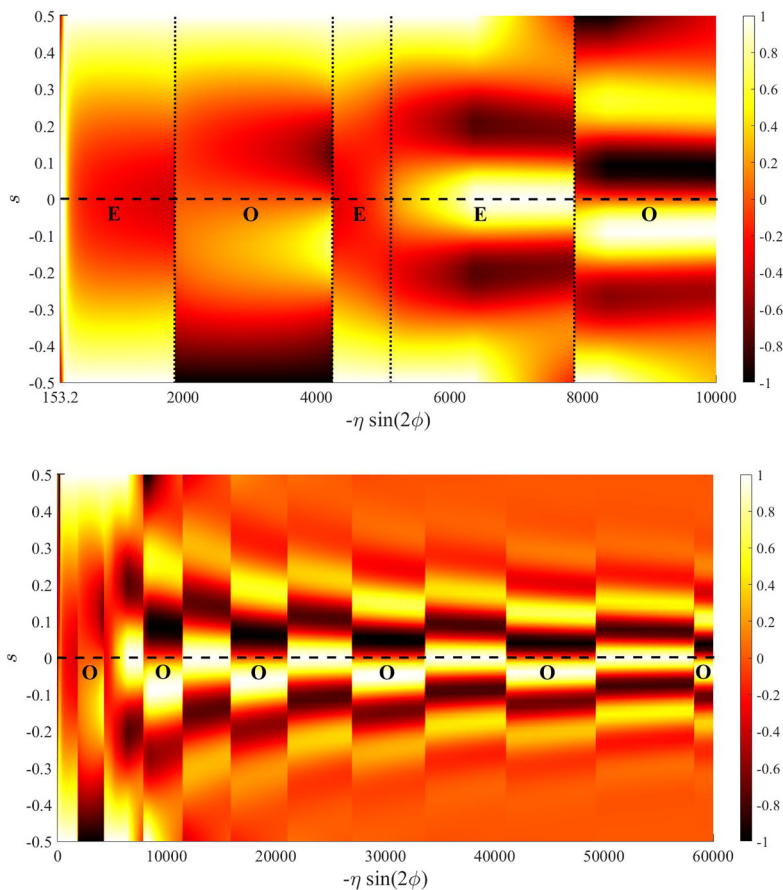
FIG. 4. The most unstable eigenfunctions $\Phi_u(s)$ are even (E) or odd (O), depending on $-\eta \sin(2\phi)$. Colors indicate values of $-1 \leqslant \Phi_u(s) \leqslant 1$. Top: The most unstable modes 1 to 5 in the lowest range of $-\eta \sin(2\phi)$, discussed in Ref. [10]. Bottom: The overview of the most unstable eigenfunctions in a wide range of $-\eta \sin(2\phi)$.

plane perturbations is smaller than the growth rate of the most unstable in-plane perturbations, as illustrated in the bottom panel of Fig. 3. The zeros of the eigenvalues σ_u and σ_v correspond to $-\eta\sin(2\phi) = \mu_1$ and μ_2, respectively, with $\mu_1 = 153.2$ and $\mu_2 = 221.2$, as shown in the bottom panel of Fig. 3. This means that the filament with an initial angle ϕ slightly smaller than π, while moving in the shear flow and decreasing the value of ϕ, will first experience in-plane instability, and later out-of-plane instability.

It is very interesting to point out that Eqs. (20) to (22) are essentially the same as Eqs. (3) and (4) in Ref. [26] for elastica in the compressional ambient flow $\boldsymbol{u} = (-x, y, 0)$, with the following modifications: instead of $\bar{\mu}$, σ, Φ_y and Φ_z from Ref. [26], here we have $-\eta \sin(2\phi)$, $-2\sigma / \sin(2\phi)$, Φ_u, and Φ_v, respectively. Therefore, if we rescale our eigenvalues σ_u by $-\sin(2\phi)/2$, a scaled eigenspectrum is obtained, shown in Fig. 6, which is the same as that illustrated by Chakrabarti *et al.* [26] in their Fig. 3(a) for their unstable planar eigenspectrum in the compressional flow. The eigenspectra in shear and compressional flows are the same.

When $-\eta \sin(2\phi)$ increases from 153.2 (a critical value at which the buckling instability occurs) to 10^4, there appear even, odd, even, even, and odd modes, respectively. When $-\eta \sin(2\phi)$ increases above 10^4, the most unstable mode still keeps alternating odd and even symmetries. This coupling
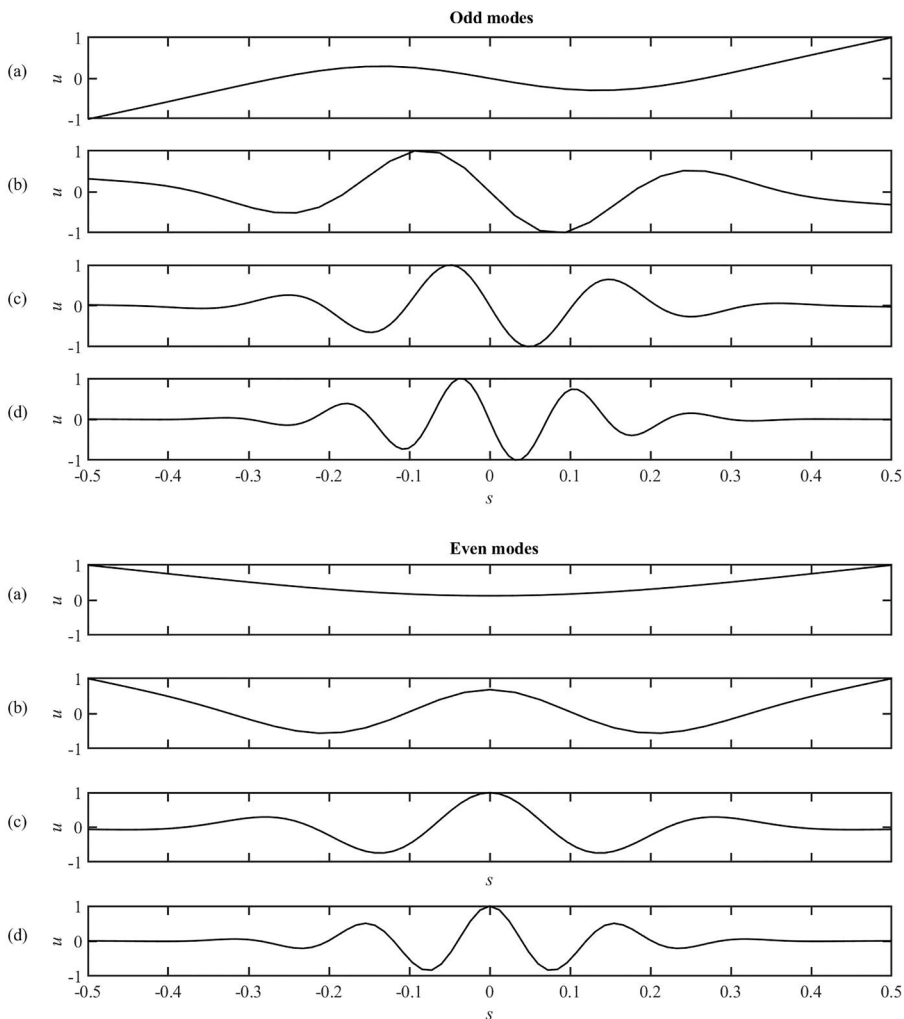
FIG. 5. Examples of the most unstable eigenfunctions $\Phi_u(s)$. Top-down: $-\eta \sin(2\phi) = 3000$ (odd mode 2), 10 000 (odd mode 5), 30 000 and 60 000 (higher odd modes), 300 (even mode 1), 6000 (even mode 4), 15 000 and 50 000 (higher even modes).

of the even and odd most unstable modes was described and shown in Fig. 3 in Ref. [26] in the context of the compressional flow.

The spectral analysis, based on Eq. (19) provides the growth rate of small perturbations from a straight shape with an arbitrary in-plane orientation λ. Figure 7 illustrates how the most unstable eigenfunctions and eigenvalues depend on the in-plane orientation, given by the angle ϕ, for a fixed value of $\eta = 10^4$. In particular, as expected, the fastest growth of small perturbations is observed for $\phi = 135°$. The unstable perturbations correspond only to angles ϕ larger than $90.44°$. Figure 7 shows that for the same value of η, shapes and parity of the most unstable eigenfunctions are in general different for different orientations. Within the spectral analysis, based on Eq. (19), the perturbation amplitude is independent of time. Keeping this in mind, nevertheless, in Fig. 7 we add time corresponding to the evolution of the orientation λ according to the zeroth order Eqs. (8) and (9). In this way, we show how a straight fiber would deform if placed at $\phi(t)$.
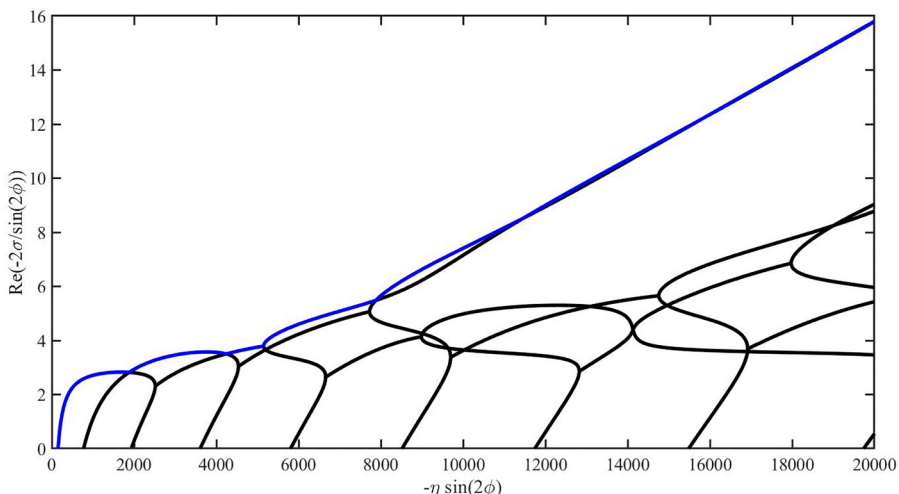
FIG. 6. Scaled eigenspectrum $\sigma = \sigma_u$ for perturbations Φ_u within the shear plane of the shear flow.

VI. CONCLUSION

In this work, we derived Eqs. (10) and (11) for the evolution of three-dimensional perturbations of a straight elastica at an arbitrary orientation. We performed spectral analysis of elastica in a shear flow, investigating perturbations out of the shear plane. We analyzed the most unstable eigenfunctions and eigenvalues.

We demonstrated that the eigenproblem for elastica in the shear flow is described by the same equations as in the compressional flow [26]. Therefore, the important conclusion from this work is that the basic features of flexible fiber dynamics in the compressional flow, found in Ref. [26], apply
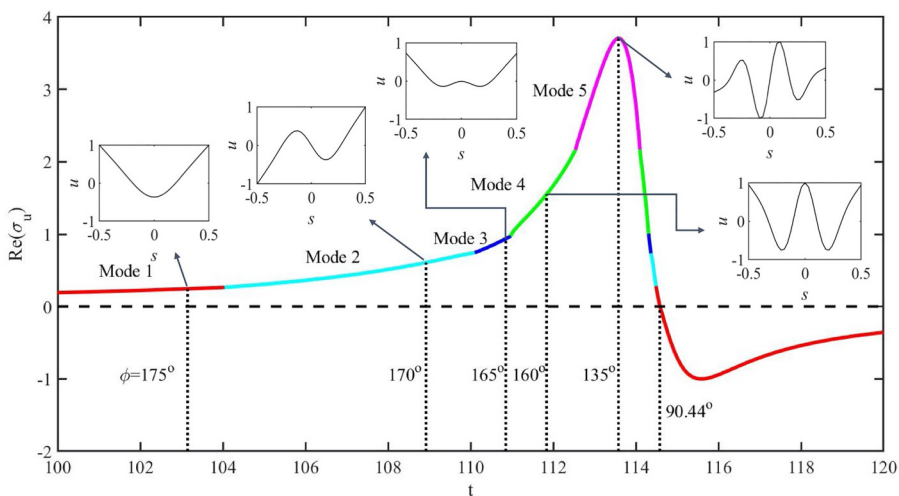

FIG. 7. The real part of the most unstable eigenvalue σ_u for the in-plane perturbations (19) of an almost straight elastica with $\eta = 10\,000$ and different orientations $\boldsymbol{\lambda}(\phi)$ at $\theta = \pi/2$. The corresponding most unstable eigenfunctions are also shown for different values of ϕ. The angle ϕ is next linked with time t according to the zero-order Eqs. (8) with $\phi = 179.5°$ at $t = 0$. The shapes shown correspond to deformations of a straight fiber at $\phi(t)$.

also in the shear flow. In particular, even though in the shear flow, the out-of-plane spectrum is just a shifted in-plane spectrum, but the coupling of both in-plane and out-of-plane eigenfunctions results in helical, 3D shapes of elastic filaments, as in the compressional flow [26]. An example of such a helical buckled elastic filament in shear flow can be found in Fig. 9 of Ref. [29].

Based on the spectral analysis presented here, in Ref. [50] scaling law for the eigenfunction shape has been derived and compared with the numerical simulations of flexible filaments made of beads. In the future, it would be interesting to extend the spectral analysis presented here and in Ref. [50] for an elastic sheet in a shear flow. Such a system was recently studied, e.g., in Refs. [51–55], with potential applications for graphene flakes.

The eigenvalues and eigenfunctions for eight most unstable modes are openly available in RepOD - Repository for Open Data at [56].

[1] A. Lindner and M. J. Shelley, Elastic fibers in flows, in *Fluid-Structure Interactions in Low Reynolds Number Flows*, edited by C. Duprat and H. A. Stone (Royal Society of Chemistry, London, 2015), pp. 168–189.

[2] O. du Roure, A. Lindner, E. N. Nazockdast, and M. J. Shelley, Dynamics of flexible fibers in viscous flows and fluids, Annu. Rev. Fluid Mech. **51**, 539 (2019).

[3] T. A. Witten and H. Diamant, A review of shaped colloidal particles in fluids: Anisotropy and chirality, Rep. Prog. Phys. **83**, 116601 (2020).

[4] O. L. Forgacs and S. G. Mason, Particle motions in sheared suspensions IX. Spin and deformation of threadlike particles, J. Colloid Sci. **14**, 457 (1959).

[5] O. L. Forgacs and S. G. Mason, Particle motions in sheared suspensions: X. Orbits of flexible threadlike particles, J. Colloid Sci. **14**, 473 (1959).

[6] P. Skjetne, R. F. Ross, and D. J. Klingenberg, Simulation of single fiber dynamics, J. Chem. Phys. **107**, 2108 (1997).

[7] J. M. Stockie and S. I. Green, Simulating the motion of flexible pulp fibres using the immersed boundary method, J. Comput. Phys. **147**, 147 (1998).

[8] S. Yamamoto and T. Matsuoka, A method for dynamic simulation of rigid and flexible fibers in a flow field, J. Chem. Phys. **98**, 644 (1993).

[9] R. M. Jendrejack, D. C. Schwartz, J. J. de Pablo, and M. D. Graham, Shear-induced migration in flowing polymer solutions: Simulation of long-chain DNA in microchannels, J. Chem. Phys. **120**, 2513 (2004).

[10] L. E. Becker and M. J. Shelley, Instability of elastic filaments in shear flow yields first-normal-stress differences, Phys. Rev. Lett. **87**, 198301 (2001).

[11] A.-K. Tornberg and M. J. Shelley, Simulating the dynamics and interactions of flexible fibers in Stokes flows, J. Comput. Phys. **196**, 8 (2004).

[12] Y.-N. Young and M. J. Shelley, Stretch-coil transition and transport of fibers in cellular flows, Phys. Rev. Lett. **99**, 058303 (2007).

[13] S. B. Lindström and T. Uesaka, Simulation of the motion of flexible fibers in viscous fluid flow, Phys. Fluids **19**, 113307 (2007).

[14] E. Wandersman, N. Quennouz, M. Fermigier, A. Lindner, and O. Du Roure, Buckled in translation, Soft Matter **6**, 5715 (2010).

[15] V. Kantsler and R. E. Goldstein, Fluctuations, dynamics, and the stretch-coil transition of single actin filaments in extensional flows, Phys. Rev. Lett. **108**, 038103 (2012).

[16] L. Guglielmini, A. Kushwaha, E. S. G. Shaqfeh, and H. A. Stone, Buckling transitions of an elastic filament in a viscous stagnation point flow, Phys. Fluids **24**, 123601 (2012).

[17] J. K. Nunes, H. Constantin, and H. A. Stone, Microfluidic tailoring of the two-dimensional morphology of crimped microfibers, Soft Matter **9**, 4227 (2013).

[18] M. Harasim, B. Wunderlich, O. Peleg, M. Kröger, and A. R. Bausch, Direct observation of the dynamics of semiflexible polymers in shear flow, Phys. Rev. Lett. **110**, 108302 (2013).

[19] K. Sinha and M. D. Graham, Dynamics of a single red blood cell in simple shear flow, Phys. Rev. E **92**, 042710 (2015).

[20] P. Nakielski, S. Pawłowska, F. Pierini, W. Liwińska, P. Hejduk, K. Zembrzycki, E. Zabost, and T. A. Kowalewski, Hydrogel nanofilaments via core-shell electrospinning, PLoS ONE **10**, e0129816 (2015).

[21] B. Delmotte, E. Climent, and F. Plouraboué, A general formulation of bead models applied to flexible fibers and active filaments at low reynolds number, J. Comput. Phys. **286**, 14 (2015).

[22] H. Manikantan and D. Saintillan, Buckling transition of a semiflexible filament in extensional flow, Phys. Rev. E **92**, 041002(R) (2015).

[23] N. Quennouz, M. Shelley, O. Du Roure, and A. Lindner, Transport and buckling dynamics of an elastic fibre in a viscous cellular flow, J. Fluid Mech. **769**, 387 (2015).

[24] Q. Yang and L. Fauci, Dynamics of a macroscopic elastic fibre in a polymeric cellular flow, J. Fluid Mech. **817**, 388 (2017).

[25] Y. Liu, B. Chakrabarti, D. Saintillan, A. Lindner, and O. Du Roure, Morphological transitions of elastic filaments in shear flow, Proc. Natl. Acad. Sci. USA **115**, 9438 (2018).

[26] B. Chakrabarti, Y. Liu, J. LaGrone, R. Cortez, L. Fauci, O. du Roure, D. Saintillan, and A. Lindner, Flexible filaments buckle into helicoidal shapes in strong compressional flows, Nat. Phys. **16**, 689 (2020).

[27] H. Nguyen and L. Fauci, Hydrodynamics of diatom chains and semiflexible fibres, J. R. Soc. Interface **11**, 20140314 (2014).

[28] E. Gauger and H. Stark, Numerical study of a microscopic artificial swimmer, Phys. Rev. E **74**, 021907 (2006).

[29] A. M. Słowicka, N. Xue, P. Sznajder, J. K. Nunes, H. A. Stone, and M. L. Ekiel-Jeżewska, Buckling of elastic fibers in a shear flow, New J. Phys. **24**, 013013 (2022).

[30] N. Autrusson, L. Guglielmini, S. Lecuyer, R. Rusconi, and H. A. Stone, The shape of an elastic filament in a two-dimensional corner flow, Phys. Fluids **23**, 063602 (2011).

[31] C. Kurzthaler, R. Brandão, O. Schnitzer, and H. A. Stone, Shape of a tethered filament in various low-Reynolds-number flows, Phys. Rev. Fluids **8**, 014101 (2023).

[32] A. M. Słowicka, E. Wajnryb, and M. L. Ekiel-Jeżewska, Dynamics of flexible fibers in shear flow, J. Chem. Phys. **143**, 124904 (2015).

[33] J. LaGrone, R. Cortez, W. Yan, and L. Fauci, Complex dynamics of long, flexible fibers in shear, J. Non-Newtonian Fluid Mech. **269**, 73 (2019).

[34] M. Kanchan and R. Maniyeri, Numerical simulation and prediction model development of multiple flexible filaments in viscous shear flow using immersed boundary method and artificial neural network techniques, Fluid Dyn. Res. **52**, 045507 (2020).

[35] A. M. Słowicka, H. A. Stone, and M. L. Ekiel-Jeżewska, Flexible fibers in shear flow approach attracting periodic solutions, Phys. Rev. E **101**, 023104 (2020).

[36] P. J. Żuk, A. M. Słowicka, M. L. Ekiel-Jeżewska, and H. A. Stone, Universal features of the shape of elastic fibres in shear flow, J. Fluid Mech. **914**, A31 (2021).

[37] N. Xue, J. K. Nunes, and H. A. Stone, Shear-induced migration of confined flexible fibers, Soft Matter **18**, 514 (2022).

[38] F. Bonacci, B. Chakrabarti, D. Saintillan, O. Du Roure, and A. Lindner, Dynamics of flexible filaments in oscillatory shear flows, J. Fluid Mech. **955**, A35 (2023).

[39] L. N. Trefethen, Chebyshev differentiation matrices, in *Spectral Methods in Matlab* (SIAM, Philadelphia, 2000), pp. 51–59.

[40] S. Timoshenko, *History of Strength of Materials* McGraw-Hill, New York, 1953).

[41] G. Batchelor, Slender-body theory for particles of arbitrary cross-section in Stokes flow, J. Fluid Mech. **44**, 419 (1970).

[42] R. G. Cox, The motion of long slender bodies in a viscous fluid Part 1. General theory, J. Fluid Mech. **44**, 791 (1970).

[43] C. Duprat and H. A. Stone, Model problems coupling elastic boundaries and viscous flows, in *Fluid-Structure Interactions in Low-Reynolds-Number Flows*, edited by C. Duprat and H. A. Stone (Royal Society of Chemistry, London, 2015), pp. 78–99.

[44] B. Audoly and Y. Pomeau, Elasticity and geometry, in *Peyresq Lectures On Nonlinear Phenomena* (World Scientific, Singapore, 2000), pp. 1–35.

[45] B. Audoly, Introduction to the elasticity of rods, in *Fluid-Structure Interactions in Low-Reynolds-Number Flows*, edited by C. Duprat and H. A. Stone (Royal Society of Chemistry, London, 2015), pp. 1–24.

[46] M. D. Graham, *Microhydrodynamics, Brownian Motion, and Complex Fluids*, Vol. 58 (Cambridge University Press, Cambridge, England, 2018).

[47] R. Cox, The motion of long slender bodies in a viscous fluid. Part 2. Shear flow, J. Fluid Mech. **45**, 625 (1971).

[48] R. E. Johnson, An improved slender-body theory for stokes flow, J. Fluid Mech. **99**, 411 (1980).

[49] J. P. Boyd, Interpolation, collocation and all that, in *Chebyshev and Fourier Spectral Methods* (Dover, New York, 2001), pp. 81–97.

[50] P. Sznajder, L. Liu, P. Zdybel, and M. L. Ekiel-Jeżewska, Scaling law for a buckled elastic filament in a shear flow, arXiv:2307.07215.

[51] M. J. Shelley and J. Zhang, Flapping and bending bodies interacting with fluid flows, Annu. Rev. Fluid Mech. **43**, 449 (2011).

[52] Y. Xu and M. J. Green, Brownian dynamics simulations of nanosheet solutions under shear, J. Chem. Phys. **141**, 024905 (2014).

[53] Y. Yu and M. D. Graham, Coil–stretch-like transition of elastic sheets in extensional flows, Soft Matter **17**, 543 (2021).

[54] K. S. Silmore, M. S. Strano, and J. W. Swan, Buckling, crumpling, and tumbling of semiflexible sheets in simple shear flow, Soft Matter **17**, 4707 (2021).

[55] G. Salussolia, C. Kamal, J. Stafford, N. Pugno, and L. Botto, Simulation of interacting elastic sheets in shear flow: Insights into buckling, sliding, and reassembly of graphene nanosheets in sheared liquids, Phys. Fluids **34**, 053311 (2022).

[56] L. Liu, P. Sznajder, and M. Ekiel-Jezewska, Eigenfunctions and eigenvalues for elastica in a shear flow (2023), https://doi.org/10.18150/USFQAK.